IEEE Access
Multidisciplinary | Rapid Review | Open Access Journal

SPECIAL SECTION ON BIG DATA LEARNING AND DISCOVERY

Received October 7, 2018, accepted October 21, 2018, date of publication October 25, 2018, date of current version November 30, 2018.

Digital Object Identifier 10.1109/ACCESS.2018.2878056

All-in-Focus Sweep Imaging Based on Wigner Distribution Function

CHANG LIU[1,2], (Member, IEEE), SHAN GAO[3], XING ZHAO[2], AND JUN QIU[1,2], (Member, IEEE)

[1]Institute of Applied Mathematics, Beijing Information Science and Technology University, Beijing 100101, China
[2]Beijing Advanced Innovation Center for Imaging Technology, Capital Normal University, Beijing 100048, China
[3]School of Science, Beijing Jiaotong University, Beijing 100044, China

Corresponding author: Jun Qiu (qiu.jun.cn@ieee.org)

This work was supported in part by the National Natural Science Foundation of China under Grant 61801031 and Grant 61871042 and in part by the Research Fund Project of Beijing Information Science and Technology University under Grant 1825025.

ABSTRACT To extend the depth of field, the all-in-focus image can be achieved via the computational imaging method by designing the data acquisition process under the condition of maintaining the signal-to-noise ratio. In this paper, the data acquisition of all-in-focus sweep imaging is described by the Wigner distribution function (WDF); then, the WDF-based all-in-focus imaging model and the computational imaging method are established. In the all-in-focus imaging model, the WDF-based light propagation model is utilized to describe the imaging process. As a consequence, the point spread function (PSF) of the imaging system is derived via the WDF-based light propagation model. By analyzing the PSF of the imaging model, the approximate 3-D spatial invariance of the PSF is achieved, and the all-in-focus sweep data can be expressed as a convolution of the all-in-focus image and the PSF. As a result, the all-in-focus image can be reconstructed by utilizing the deconvolution in the computational imaging. In the simulated experiments, the computational imaging results in different object planes are analyzed based on the structural similarity index to verify the all-in-focus sweep imaging method. In the real data experiments, the resolution targets placed in two different depths can be imaged with extended depth of field via the all-in-focus imaging method proposed in this paper.

INDEX TERMS Computational imaging, extended depth of field, focal sweep, Wigner distribution function.

I. INTRODUCTION

Since the PSF depends on the depth of the imaging plane, the depth of field in the lens imaging is limited. It is often necessary to decrease the aperture to extend the depth of field. However, the decrease of the aperture leads to the decrease of the total light flux, resulting in a lower signal-to-noise ratio of the image. How to obtain the image with extended depth of field and acceptable signal-to-noise ratio is a hot topic in the field of computational imaging. By designing the optical path of the imaging system, the AIF imaging obtains the raw data containing a wealth of scene information and recontructs the sharp image within the large depth of field by the post computaional imaging. Compared with the conventional lens imaging, the all-in-focus imaging provides richer and more effective data for object recognition, scene reconstruction and scene stitching [1], [2].

The approaches of implementing the all-in-focus imaging are composed of the design of the structured PSF on the pupil plane and the sweep of the imaging plane. The means of designing the PSF on the pupil plane includes wavefront coding [3]–[13] and coded aperture [14]–[16], which require the change of the lens or inserting the mask into the imaging system. The coded aperture imaging leads to the decrease in the total amount of light flux via the imaging system, resulting in the decrease of the signal-to-noise ratio. The sweep of the imaging plane is to obtain the focus sweep [17]–[19] data or the focal stack [20]–[22] data. The PSF of the focal sweep data is achieved with the approximate depth invariance by sweeping the imaging plane in a certain depth range during the exposure time. The focal stack data is a set of images that are focused on different planes. The sweeping approach can be implemented via the translation of the imaging plane rather than the insertion of new optics, and enables flexible acquisition of real scenes. To analyze the PSF of all-in-focus sweep imaging, the existing studies have verified that the PSF is approximately depth invariant from the derivation by the

geometric optics and the experimental evaluation. Since the derivation based on geometric optics approximates the optical radiation to geometrical light by ignoring its wave characteristics, the description of the full-focus scanning imaging is incomplete.

As a characterization of generalized radiant energy, WDF uses Fourier optics and time-frequency analysis to describe the light field more completely. Therefore, WDF can be applied to model the optical imaging system. The WDF of optical radiation characterizes the joint distribution of spatial and frequency to provide a complete description of beam characteristics. In addition, WDF has reflection symmetry including time symmetry and spatial symmetry, which is widely used in image processing. As an effective time-frequency analysis method, WDF can be utilized to establish the light field imaging model and inverse problem to realize the high-precision all-in-focus imaging algorithm. In this paper, we apply the WDF as a tool to model the all-in-focus sweep imaging system, and to analyze the approximate 3D invariance of the PSF of the all-in-focus sweep imaging and establish the all-in-focus computational imaging method.

The WDF [23] has become a powerful tool for analyzing optical imaging systems. The WDF can describe intensity and angular spectrum information under the condition of the paraxial approximation, and can model the light propagation in free space and the diffraction effect of the aperture in the imaging system. In this paper, the WDF is applied to model the all-in-focus sweep imaging and establish the 3D deconvolution computational imaging method of all-in-focus sweep imaging by the relationship between the WDF and the PSF. The results of this paper provide theoretical basis for further design of all-in-focus sweep imaging model.

II. RELATED WORKS

The PSF of the lens imaging depends on the depth of the imaging plane, the large aperture leads to the limited depth of field, while the small aperture results in the low signal-to-noise ratio of the image. The focal sweep imaging is an effective computational imaging method to obtain the image with large depth of field. The all-in-focus image can be achieved via the computational imaging method by acquiring images with the same degree of blur. As shown in FIGURE 1, the focal sweep system obtains the accumulated images of different depths by translating the imaging plane during the exposure time, and the focal stack system captures a set of images in different depths by translating the imaging plane. In FIGURE 1, D is the diameter of the lens, d_0 is the depth of the scene point, s_0 is conjugated with d_0, and the scanning range is $\Delta s = s_{max} - s_{min}$. With the focal length f, Gaussian imaging formula is expressed as

$$\frac{1}{d_0} + \frac{1}{s_0} = \frac{1}{f} \tag{1}$$

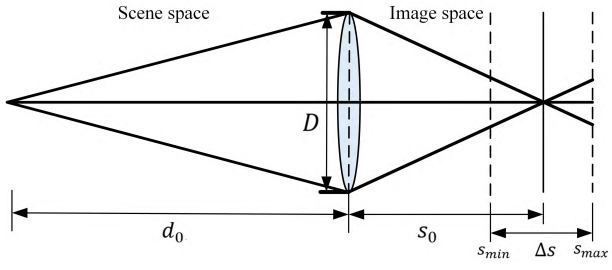

FIGURE 1. Diagram of all-in-focus sweep imaging system.

The all-in-focus sweep imaging models can be divided into two categories: non-mechanical and mechanical focal sweep imaging models. The no-mechanical model is to obtain the image with the same degree of blur by changing the focal length of the lens. Miau *et al.* proposed a telephoto camera with a varifocal lens for video refocusing and trajectory tracking of the moving object. The model of mechanical motion obtains the image with approximately the same degree of blur by translating the position of the sensor plane or translating the lens plane during the exposure. Nagahara *et al.* [24] proposed the method of mechanical motion, which expands the depth of field by translating the sensor during the exposure, and gave the experimental analysis of the approximate depth invariance of integration point spread function (IPSF). Yokoya and Nayar [25] obtained the wide viewing angle, near-invariant imaging system by adding the curved mirror. Lin *et al.* [26] implemented a coded focal stack design by controlling the exposure time of each pixel. Kubota *et al.* [27] modeled the multiple views and the desired all-in-focus view as a set of linear equations with a combination of textures at the focal depths. Iwai *et al.* [28] proposed a fast focal sweep method with the focus tunable lens (FTL) projector.

The existing description and analysis of the focal sweep imaging model is based on the geometric optics, by establishing a PSF with the approximate depth invariance and using this PSF to compute the image by the deconvolution method. The WDF expands the light propagation from the geometric optics category to the wave optics category, providing a new tool for the description of the imaging system. The application of the WDF to optical imaging enables computational imaging to maintain the computational simplicity of geometric optics, and also includes certain wave optics properties. We propose the description of the all-in-focus sweep imaging model based on the WDF, derive the PSF of all-in-focus sweep imaging based on the WDF, and establish the computational imaging method to achieve the all-in-focus image.

The WDF is the characterization of the joint distribution of spatial position and frequency. Zhang and Levoy proposed to use the WDF to represent the optical radiation distribution of the wave field. It was proved that the light field approximates to the Wigner distribution under geometric optical approximation, which was equal to the smoothed Wigner distribution. The characterization of the light field was extended to coherent optical radiation and the extended light field was used to interpret the formation of the coherent image [29]. Oh *et al.* proposed the concept of augmented light field

based on the WDF, and obtained the Wigner distribution representation of amplitude and phase optics. The formula for enhancing the propagation of the light field in the optics was also given [30]. Cuypers *et al.* [31] elaborated on the relationship between the Wigner distribution and the phase space, and demonstrated that the Wigner distribution was used to simulate the diffraction effects, and discussed the effectiveness of the WDF in near-field, far-field and paraxial approximations. These studies provide theoretical support for the WDF-based light description models.

III. ALL-IN-FOCUS SWEEP IMAGING BASED ON THE WDF

A. WDF OF THE WAVEFRONT SIGNAL

The WDF of the signal $t(x, y)$ is denoted as $W_t(x, y, u, v)$

$$W_t(x, y, u, v) = \iint J(x, y, x', y') \exp(-i2\pi(x'u + y'v))dx'dy' \tag{2}$$

where $J(x, y, x', y') = t(x + \frac{x'}{2}, y + \frac{y'}{2})t^*(x - \frac{x'}{2}, y - \frac{y'}{2})$, and $W_t(x, y, u,)$ is the quadratic time-frequency distribution.

The WDF of the sum of the signal $f(x, y)$ and $g(x, y)$ is

$$\begin{aligned} W_{f+g}(x, y, u, v) &= W_f(x, y, u, v) + W_g(x, y, u, v) \\ &\quad + 2ReW_{f,g}(x, y, u, v) \end{aligned} \tag{3}$$

Here, $2ReW_{f,g}(x, y, u, v)$ represents a cross term of the signal $f(x, y)$ and $g(x, y)$. The cross term can describe the interference phenomenon. For example, the WFD of $t(x, y) = \delta(x - a) + \delta(x - b)$ in Young's double-slit interference is

$$\begin{aligned} W_t(x, y, u, v) &= \delta(x - a) + \delta(x - b) \\ &\quad + \delta(x - \frac{a + b}{2}) \cos(2\pi |a - b|u) \end{aligned} \tag{4}$$

The WFD Marginals represent the angular spectrum $|\widetilde{t}(u, v)|^2$ of the plane wave and the intensity $|t(x, y)|^2$ on the imaging plane.

$$|t(u, v)|^2 = \iint W_t(x, y, u, v)dudv \tag{5}$$

$$|\widetilde{t}(u, v)|^2 = \iint W_t(x, y, u, v)dxdy \tag{6}$$

From the angular spectrum representation of wave optics, the wavefront represented by the complex amplitude $t(x, y)$ can be decomposed by Fourier series into the plane wave $\widetilde{t}(u, v)$ with the frequency component of $\widetilde{t}(u, v) \exp(i2\pi(ux + yv))$. Assuming that the direction cosine of the plane wave is $(\cos(\alpha), \cos(\beta))$, then

$$\begin{aligned} &\widetilde{t}(u, v) \exp(ik(x \cos(\alpha) + y \sin(\beta))) \\ &\quad = \widetilde{t}(u, v) \exp(i2\pi(ux + yv)) \end{aligned} \tag{7}$$

where k is the wave vector and $k = 2\pi/\lambda$. Considering the plane wave as a set of parallel rays, the angles α, β of the parallel rays satisfy

$$u = \frac{\cos(\alpha)}{\lambda}, \quad v = \frac{\cos(\beta)}{\lambda} \tag{8}$$

Therefore, $W_t(x, y, u, v)$ can be regarded as the energy distribution of the light beam at the position (x, y) with the angle $\alpha = \cos^{-1}(\lambda u)$, $\beta = \cos^{-1}(\lambda v)$.

B. LIGHT PROPAGATION MODEL BASED ON WFD

In the linear optics, the light waves propagating through the optical system can be expressed as an integral equation by using the integral kernel [32]. The two-dimensional complex amplitude $t_in(x, y)$ can be expressed as

$$t_{out}(s, t) = \iint t_{in}(x, y)h(x, y, s, t)dxdy \tag{9}$$

where (x, y) and (s, t) are the coordinates of the input and output planes respectively, and $t_{out}(s, t)$ and $t_{in}(x, y)$ represent the complex amplitudes of the output and input planes respectively. $h(x, y, s, t)$ is the transfer function between the input plane and the output plane.

We consider that the light wave propagates in free space. By the Fresnel approximation, $h(x, y, s, t)$ can be expressed as

$$h(x, y, s, t) = \frac{\exp(i\frac{2\pi}{\lambda}z)}{i\lambda} \exp(i\frac{\pi}{\lambda z}(s - x)^2 + (t - y)^2)dxdy \tag{10}$$

After the propagation by the distance z in free space, the WDF at the output plane is obtained.

$$W_{out}(s, t, u, v) = W_{in}(s - \lambda uz, t - \lambda vz, u, v) \tag{11}$$

For the lens imaging, $h(x, y, s, t)$ of the thin lens under paraxial approximation is

$$h(x, y, s, t) = \exp(-i\frac{\pi}{\lambda f}(x^2 + y^2))\delta(s - x, t - y) \tag{12}$$

After passing through the lens, the WFD at the output plane is obtained.

$$W_{out}(s, t, u, v) = W_{in}(s, u + us\frac{k}{f}, t, v + vt\frac{k}{f}) \tag{13}$$

For the aperture or the mask, the complex amplitude in the output plane is the modulation of the input plane by the function $m(x, y)$.

$$t_{out}(x, y) = t_{in}(x, y)m(x, y) \tag{14}$$

The multiplication in the spatial domain is equivalent to convolution in the frequency domain. Therefore, the WDF of the output plane is represented by the convolution of the $W(x, y, u, v)$ and $W_m(x, y, u, v)$ with respect to the frequency domain.

$$\begin{aligned} &W_{out}(x, y, u, v) \\ &\quad = \iint W_{in}(x, y, u - a, v - b)W_m(x, y, a, b)dadb \end{aligned} \tag{15}$$

For the image on the imaging plane, the intensity $I(x, y)$ is the integral value of the light intensity about the direction (u, v) described by $W(x, y, u, v)$, as known by (5).

$$I(x, y) = \iint W(x, y, u, v)dudv \tag{16}$$

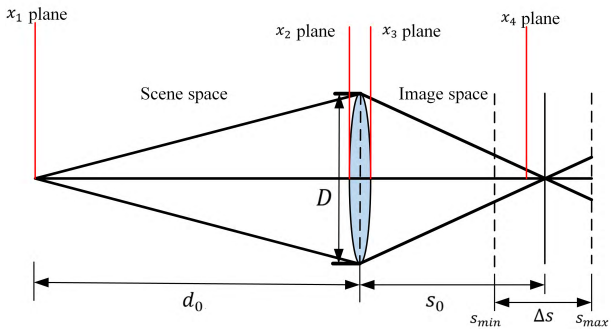

FIGURE 2. Diagram of different planes in the WFD based light propagation model.

IV. ALL-IN-FOCUS SWEEP IMAGING MODEL AND COMPUTATIONAL IMAGING METHOD

A. ALL-IN-FOCUS SWEEP IMAGING MODEL

According to the WFD based light propagation model, the data acquisition process of the focal stack and the focal sweep can be described. We consider the one-dimensional complex amplitude of the wavefront and derive the PSFs of the focal stack and the focal sweep. The two-dimensional complex amplitude of the wavefront can be extended from one dimension.

Let the object point be a pulse function $\delta(x-x_0)$. The WDF in the of the object plane $x_1 - plane$ is

$$\begin{aligned} W_1(x,u) &= \int t(x+\frac{x'}{2})t^*(x-\frac{x'}{2})\exp(-2\pi i x'u)dx' \\ &= \int \delta(x+\frac{x'}{2}-x_0)\delta(x-\frac{x'}{2}-x_0) \\ &\quad \times \exp(-2\pi i x'u)dx' \\ &= \int \delta(x-x_0)\delta(x')\exp(-2\pi i x'u)dx' \\ &= \delta(x-x_0) \end{aligned} \tag{17}$$

Propagating from the object plane $x_1 - plane$ to the lens input plane $x_2 - plane$ is described by (11). Then the propagation distance is d_0 and the WDF on $x_2 - plane$ is obtained.

$$W_2'(x,u) = W_1(x-\lambda d_0 u, u) \tag{18}$$

The WDF passing through the pupil function $R(x) = \begin{cases} 1, & |x| \le \frac{D}{2} \\ 0, & \text{others} \end{cases}$ on the lens input plane is

$$W_R(x,u) = 2(D-2|x|)sinc\{2(D-2|x|)u\} \tag{19}$$

Therefore, the WDF on $x_2 - plane$ after the pupil function is

$$\begin{aligned} W_2(x,u) &= W_2'(x,u) * W_R(x,u) \\ &= \int \delta(x-x_0-\lambda d_0\xi)W_R(x,u-\xi)d\xi \\ &= \int \delta(x-x_0-\lambda d_0\xi)2(D-2|x|) \\ &\quad \times sinc\{2(D-2|x|)(u-\xi)\}d\xi \\ &= \frac{2}{\lambda d_0}(D-2|x|) \\ &\quad \times sinc\{2(D-2|x|)(u-\frac{1}{\lambda d_0}(x-x_0))\} \end{aligned} \tag{20}$$

After passing through the lens, the WDF on the lens output plane $x_3 - plane$ is obtained by (13).

$$\begin{aligned} W_3(x,u) &= W_2(x,u+\frac{1}{\lambda f}x) \\ &= \frac{2}{\lambda d_0}(D-2|x|)sinc\{2(D-2|x|) \\ &\quad \times (u+\frac{1}{\lambda f}x-\frac{1}{\lambda d_0}(x-x_0))\} \end{aligned} \tag{21}$$

Propagating from $x_3 - plane$ to the imaging plane $x_4 - plane$ by the distance of s. Described by (11), the WDF at $x_4 - plane$ is

$$\begin{aligned} W_4(x,u) &= W_3(x-\lambda u d_0, u_2) \\ &= \frac{2}{\lambda d_0}(D-2|x-\lambda u d_0|)sinc\{2(D-2|x-\lambda u d_0|) \\ &\quad \times (u+\frac{1}{\lambda f}(x-\lambda u d_0)-\frac{1}{\lambda d_0}(x-\lambda u d_0-x_0))\} \end{aligned} \tag{22}$$

Therefore, the PSF of the object point at a distance d_0 is

$$\begin{aligned} PSF_s(x) = \int_{u_1}^{u_2} &\frac{2}{\lambda s}(D-2|x-\lambda u s|)sinc\{2(D-2|x-\lambda u s|) \\ &\times (u+\frac{1}{\lambda f}(x-\lambda u s)-\frac{1}{\lambda d_0}(x-\lambda u s-x_0))\}du \end{aligned} \tag{23}$$

where $u_1 = -\frac{\arctan\frac{D}{2d_0}}{\lambda}$ and $u_2 = \frac{\arctan\frac{D}{2d_0}}{\lambda}$ are the upper and lower limits of the integral. $PSF_s(x)$ is the PSF on the imaging plane.

The PSF of all-in-focus sweep imaging with the sweep range $[s_{min}, s_{max}]$ is

$$PSF(x) = \int_{s_{max}}^{s_{min}} PSF_s(x)ds \tag{24}$$

B. APPROXIMATE 3D INVARIANCE OF PSF OF ALL-IN-FOCUS SWEEP IMAGING MODEL

The 3D invariance of the imaging system's PSF means that the PSFs corresponding to the object points at different depths and different positions are approximately the same. According to the PSFs of the conventional lens imaging and the all-in-focus imaging derived based on the WFD, the PSFs in different object planes are analyzed and compared in this subsection. The analysis yields the PSF of all-in-focus sweep imaging model has approximately 3D invariance.

Set the parameters of the all-in-focus imaging model to be $f = 12.5\ mm$, $f/1.4$ and $\triangle s = 0.36\ mm$. The PSFs of the conventional lens imaging and the all-in-focus sweep imaging at different imaging planes are given below, and the

approximate 3D spatial invariance of the all-in-focus sweep imaging model's PSF is shown.

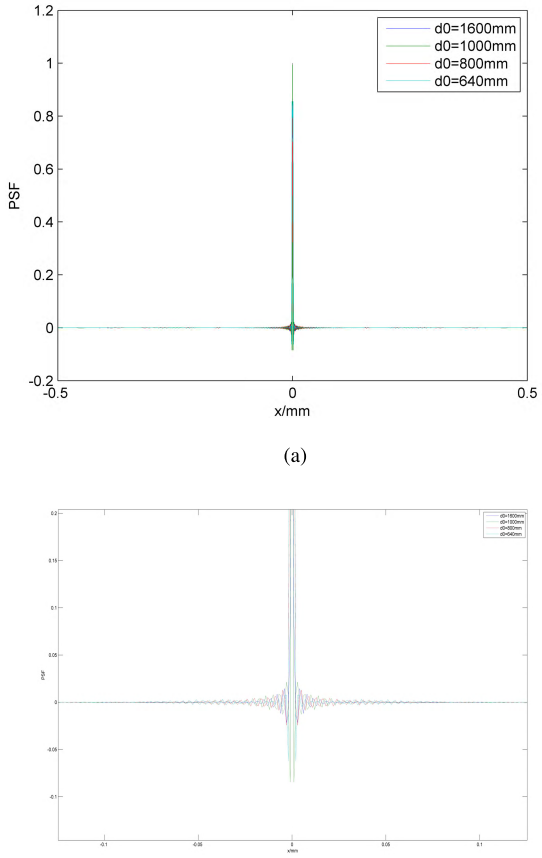

FIGURE 3. PSFs of the conventional lens imaging system. The curves of different colors represent the PSF corresponding to different object point depths ($d_0 = 1600mm$, $1000mm$, $800mm$ and $640mm$). It can be seen that the PSFs of different depths are quite different. (a) PSFs of the imaging system. (b) close-up of (a).

As shown in FIGURE 3, the PSF of the conventional lens imaging system varies greatly with depth. As shown in FIGURE 4, the PSF of the all-in-focus sweep imaging system is insensitive to the changes in depth, and the PSF of different object points on the plane at the same depth are the same as each other. Therefore, the PSF of the all-in-focus sweep imaging system has an approximate 3D spatial invariance.

C. DECONVOLUTION FOR ALL-IN-FOCUS IMAGING

By analyzing the PSF in the imaging model, the approximate three-dimensional spatial invariance of the PSF is obtained. Since the all-in-focus image is formed by all the focused points, the data $S(x, y)$ obtained by the all-in-focus sweep system can be regarded as the two-dimensional convolution of the all-in-focus image $AIF(x, y)$ and $PSF(x, y)$ of the imaging system.

$$S(x, y) = AIF(x, y) * PSF(x, y) \tag{25}$$

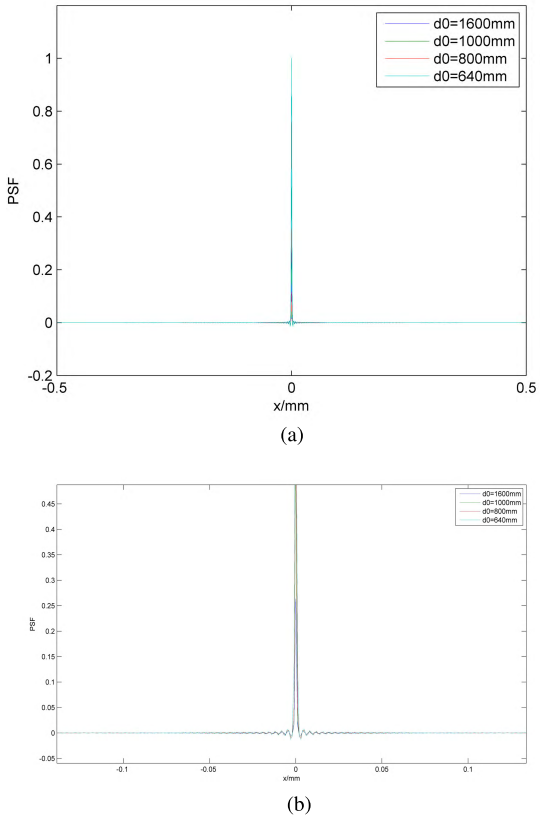

FIGURE 4. PSFs of the all-in-focus sweep imaging system. The curves of different colors represent the PSF corresponding to different object point depths ($d_0 = 1600mm$, $1000mm$, $800mm$ and $640mm$). It can be seen that the PSFs of different depths are substantially the same.(a) PSFs of the imaging system. (b) close-up of (a).

In the computational imaging process, the deconvolution mothed can be utilized via the PSF to obtain the all-in-focus image.

V. EXPERIMENTAL RESULTS

The simulated data and the real data were used to verify the proposed model and computational imaging method. The simulation experiment used the resolution target USAF 1951 with a resolution of 215×208. The resolution target was set at three different object planes, and the all-in-focus sweep data was captured with the same sweep range $[s_{min}, s_{max}]$ on the image side. The deconvolution for all-in-focus imaging was realized by Wiener filter based on the derived PSF. In the real data experiment, two resolution plates were placed at different depths, and the all-in-focus sweep data was obtained by multipling focal stack data. In the computational imaging, the PSF derived from the real imaging system was used to obtain images in which the two resolution plates are clearly imaged.

A. THE SIMULATION EXPERIMENT

In order to compare with the conventional lens imaging system, the imaging results of the conventional lens imaging system on different imaging planes were simulated and

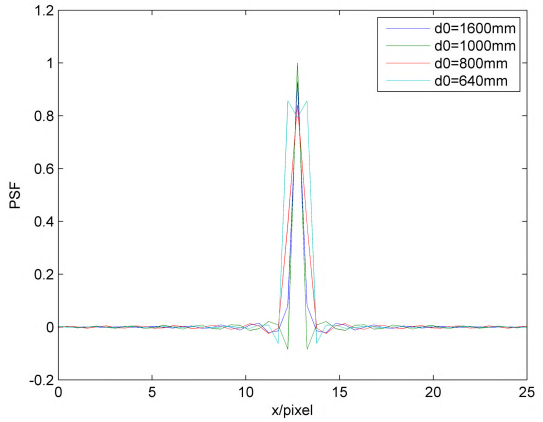

FIGURE 5. PSFs of the conventional lens imaging for the simulated experiment (The pixel size is set to be $2\mu m$).

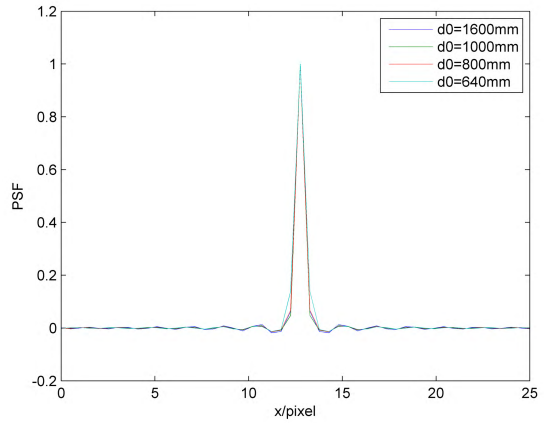

FIGURE 6. PSFs of the all-in-focus sweep imaging for the simulated experiment (The pixel size is set to be $2\mu m$).

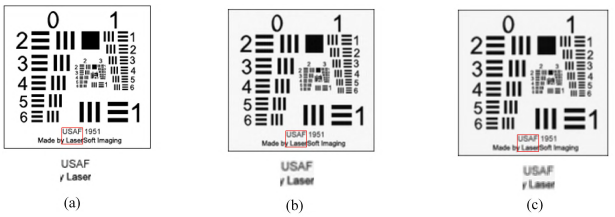

FIGURE 7. Images of a conventional imaging system in different imaging planes ($d_0 = 1600mm, 1000mm, 640mm$). It can be seen that the sharpness of the image differs greatly.

analyzed firstly. The PSFs for the simulated experiment are 25×25 pixels truncated from FIGURE 3 and FIGURE 4. Then, the all-in-focus sweep imaging data were simulated to obtain the blurred image, and the all-in-focus images were achieved by the deconvolution method.

The simulation experiments show that the conventional lens imaging system has different degrees of image blur when the imaging plane changes. The all-in-focus sweep model has approximate 3D spatial invariance, and the image with the

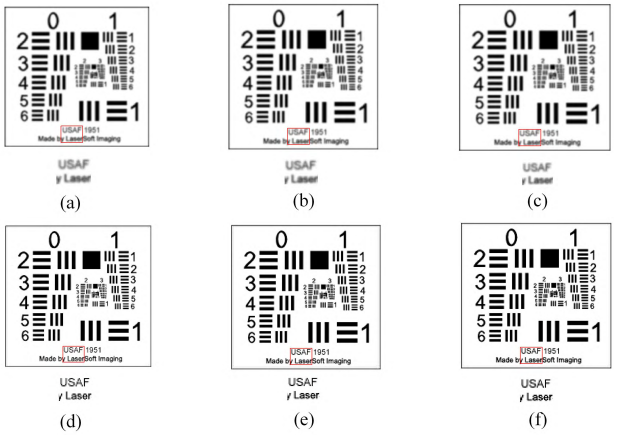

FIGURE 8. Blurred images (a-c) in different planes ($d_0 = 1600mm$, $1000mm$, $640mm$) obtained by the all-in-focus sweep system, and the all-in-focus images (d-f) obtained via the computational imaging. It can be seen that the reconstructed image details are clearer and the sharpness is basically the same.

same degree of blur can be obtained. The sharp images can be obtained by the deconvolution method for the computational imaging.

In this paper, the structural similarity index metric (SSIM) [33] is used to analyze the imaging results in different imaging planes. The SSIM index measures the similarity between two images, which is a quality measure of one of the images with the other one regarding as of perfect quality. It has reference value for the reconstruction ability of reconstruction algorithm. SSIM ranges from -1 to 1. When the two images are identical, the value of SSIM is equal to 1. SSIM is defined as

$$SSIM(x, y) = \frac{(2\mu_x\mu_y + c_1)(2\sigma_{xy} + c_2)}{(\mu_x^2 + \mu_y^2 + c_1)(\sigma_x^2 + \sigma_y^2 + c_2)} \tag{26}$$

where μ_x is the average of x, μ_y is the average of y, σ_x^2 the variance of x, $sigma_y^2$ the variance of y, σ_{xy} the covariance of x and y. $c_1 = (k_1 L)^2$, $c_2 = (k_2 L)^2$ are two variables to stabilize the division with weak denominator. L is the dynamic range of the pixel values. $k_1 = 0.01$ and $k_2 = 0.03$ by default.

The SSIM of 10 images with distance sampling interval of 0.01 mm are plotted. The range of the distance from the image to the main lens is $s \in [12.475, 12.565]mm$. The image quality at the ends of the image is declining, as shown in FIGURE 9.

B. THE REAL DATA EXPERIMENT

The experimental platform for verifying the all-in-focus imaging system was set up. The all-in-focus sweep data was obtained by fusing the focal stack data. The all-in-focus image of the real scene by the deconvolution mothed using the derived PSF according to the imaging system parameters. We used the Point Grey camera ($modelGS3 - U3 - 60S6M - C$) and Myutron prime lens ($modelHF5018V$) with the f number of $f/2$.

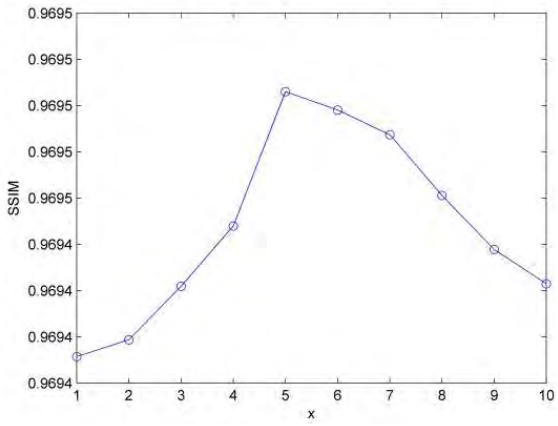

FIGURE 9. SSIM of imaging results of the resolution plate in different object plane. The SSIM value at both ends of the image is decreasing.

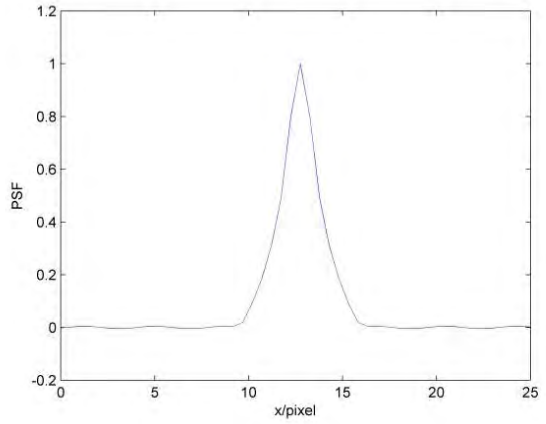

FIGURE 10. PSF of the all-in-focus sweep imaging system derived via the system parameters.

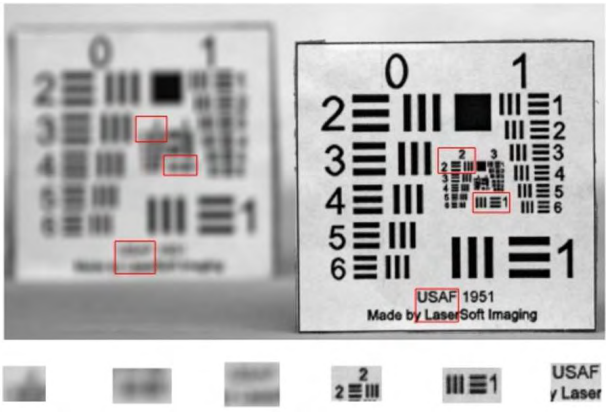

FIGURE 11. The image of the conventional camera focuses on the first resolution plate. The first resolution plate has clear imaging details.

It can be obtained from the figure that the all-in-focus image with the extended depth of field can be obtained by the proposed method, which verifies the feasibility and effectiveness.

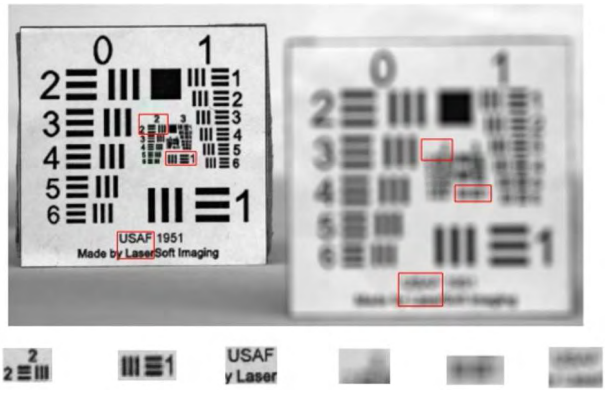

FIGURE 12. The image of the conventional camera focuses on the second resolution plate. The second resolution plate has clear imaging details.

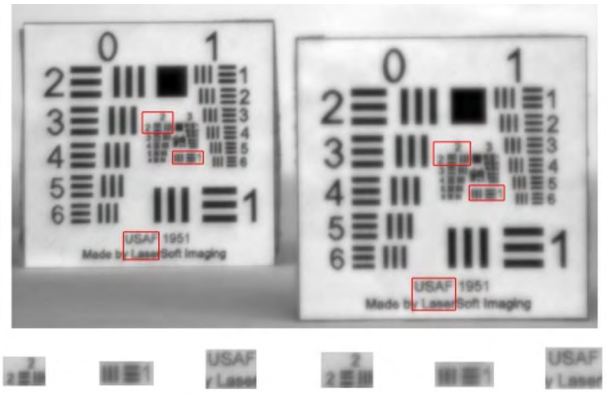

FIGURE 13. The blurred image obtained by all-in-focus sweep imaging. Both resolution plates are blurred.

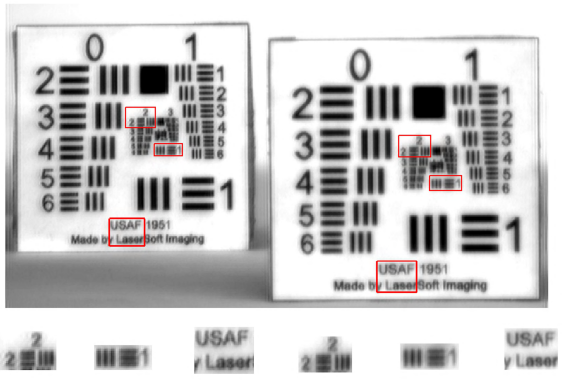

FIGURE 14. The all-in-focus image via the computational imaging based on Wigner distribution function. The imaging details of both resolution plates are clear.

VI. SUMMARY

In this paper, the Wigner distribution function is utilized to describe the all-in-focus sweep imaging system, and the WDF based all-in-focus imaging model and the computational imaging method are established. The PSF of the imaging system is derived based on the WDF based

imaging model. By analyzing the approximate 3D spatial invariance of the PSF of the imaging system, the all-in-focus imaging is realized by the deconvolution method. This method provides a theoretical basis for the depth-of-field performance analysis and sweep range selection of the all-in-focus imaging model. This method can be further applied to the analysis of other depth-of-field imaging systems.

Taking the Wigner distribution function as the tool of modeling and analyzing the imaging system, the computational imaging maintains the computational simplicity of geometric optics, and also contains certain wave optical properties. And the intrinsic relationship between the WDF and the light field computational imaging is the foundation to construct the parametric representation of the light field under the WDF and establish the light field computational imaging model based on the light field data parameterized by the WDF.

The Wigner distribution function can extend the geometric optics based light field and explore new light field imaging models, which can provide new ideas for existing light field imaging technology. The high-precision scene depth reconstruction and all-in-focus imaging algorithm can be realized by establishing the light field imaging model, inverse problem and regularization solution via Wigner distribution function. The light field imaging model will be introduced to establish the novel light field data acquisition mode, computational imaging method, and related applications.

REFERENCES

[1] C. Zhou and S. K. Nayar, "Computational cameras: Convergence of optics and processing," *IEEE Trans. Image Process.*, vol. 20, no. 12, pp. 3322–3340, Dec. 2011.

[2] O. Cossairt, M. Gupta, and S. K. Nayar, "When does computational imaging improve performance?" *IEEE Trans. Image Process.*, vol. 22, no. 2, pp. 447–458, Feb. 2013.

[3] E. R. Dowski and W. T. Cathey, "Extended depth of field through wavefront coding," *Appl. Opt.*, vol. 34, no. 11, pp. 1859–1866, 1995.

[4] S. S. Sherif, E. R. Dowski, and W. T. Cathey, "Logarithmic phase filter to extend the depth of field of incoherent hybrid imaging systems," *Proc. SPIE*, vol. 4471, pp. 272–281, Nov. 2001.

[5] W. Chi and N. George, "Electronic imaging using a logarithmic asphere," *Opt. Lett.*, vol. 26, no. 12, pp. 875–877, 2001.

[6] K. Kubala, E. Dowski, and W. T. Cathey, "Reducing complexity in computational imaging systems," *Opt. Express*, vol. 11, no. 18, pp. 2102–2108, 2003.

[7] S. Prasad, T. C. Torgersen, V. P. Pauca, R. J. Plemmons, and J. van der Gracht, "Engineering the pupil phase to improve image quality," *Proc. SPIE*, vol. 5108, pp. 1–13, Aug. 2003.

[8] V. P. Pauca, R. J. Plemmons, S. Prasad, T. C. Torgersen, and J. van der Gracht, "Integrated optical-digital approaches for enhancing image restoration and focus invariance," *Proc. SPIE*, vol. 5205, pp. 348–358, Dec. 2003.

[9] S. Prasad, T. C. Torgersen, V. P. Pauca, R. J. Plemmons, and J. van der Gracht, "High-resolution imaging using integrated optical systems," *Int. J. Imag. Syst. Technol.*, vol. 14, no. 2, pp. 67–74, 2004.

[10] A. Castro and J. Ojeda-Castaneda, "Increased depth of field with phase-only filters: Ambiguity function," *Proc. SPIE*, vol. 5827, pp. 1–12, Jun. 2005.

[11] M. Somayaji and M. P. Christensen, "Frequency analysis of the wavefront-coding odd-symmetric quadratic phase mask," *Appl. Opt.*, vol. 46, no. 2, pp. 216–226, 2007.

[12] S. R. Gottesman and E. E. Fenimore, "New family of binary arrays for coded aperture imaging," *Appl. Opt.*, vol. 28, no. 20, pp. 4344–4352, 1989.

[13] R. Raskar, A. Agrawal, and J. Tumblin, "Coded exposure photography: Motion deblurring using fluttered shutter," *ACM Trans. Graph.*, vol. 25, no. 3, pp. 795–804, Jul. 2006.

[14] A. Levin, R. Fergus, F. Durand, and W. T. Freeman, "Image and depth from a conventional camera with a coded aperture," *ACM Trans. Graph.*, vol. 26, no. 3, 2007, Art. no. 70.

[15] A. Veeraraghavan, R. Raskar, A. Agrawal, A. Mohan, and J. Tumblin, "Dappled photography: Mask enhanced cameras for heterodyned light fields and coded aperture refocusing," *ACM Trans. Graph.*, vol. 26, no. 3, 2007, Art. no. 69.

[16] C. Zhou and S. Nayar, "What are good apertures for defocus deblurring?" in *Proc. IEEE Int. Conf. Comput. Photography (ICCP)*, Apr. 2009, pp. 1–8.

[17] G. Häusler, "A method to increase the depth of focus by two step image processing," *Opt. Commun.*, vol. 6, no. 1, pp. 38–42, 1972.

[18] S. Liu and H. Hua, "Extended depth-of-field microscopic imaging with a variable focus microscope objective," *Opt. Express*, vol. 19, no. 1, pp. 353–362, 2011.

[19] C. Zhou, D. Miau, and S. K. Nayar, "Focal sweep camera for space-time refocusing," Dept. Comput. Sci., Columbia Univ., New York, NY, USA, Tech. Rep. CUCS-021-12, 2012.

[20] S. W. Hasinoff and K. N. Kutulakos, "Confocal stereo," in *Proc. ECCV*. New York, NY, USA: Springer, 2006, pp. 620–634.

[21] S. W. Hasinoff and K. N. Kutulakos, "Light-efficient photography," *IEEE Trans. Pattern Anal. Mach. Intell.*, vol. 33, no. 11, pp. 2203–2214, Nov. 2011.

[22] K. N. Kutulakos and S. W. Hasinoff, "Focal stack photography: High-performance photography with a conventional camera.," in *Proc. MVA*, 2009, pp. 332–337.

[23] E. P. Wigner, "On the quantum correction for thermodynamic equilibrium," in *Part I: Physical Chemistry. Part II: Solid State Physics*. New York, NY, USA: Springer, 1997, pp. 110–120.

[24] H. Nagahara, S. Kuthirummal, C. Zhou, and S. K. Nayar, "Flexible depth of field photography," in *Proc. Eur. Conf. Comput. Vis.* New York, NY, USA: Springer, 2008, pp. 60–73.

[25] R. Yokoya and S. K. Nayar, "Extended depth of field catadioptric imaging using focal sweep," in *Proc. IEEE Int. Conf. Comput. Vis.*, Dec. 2015, pp. 3505–3513.

[26] X. Lin, J. Suo, G. Wetzstein, Q. Dai, and R. Raskar, "Coded focal stack photography," in *Proc. IEEE Int. Conf. Comput. Photogr. (ICCP)*, Apr. 2013, pp. 1–9.

[27] A. Kubota, K. Aizawa, and T. Chen, "Reconstructing dense light field from array of multifocus images for novel view synthesis," *IEEE Trans. Image Process.*, vol. 16, no. 1, pp. 269–279, Jan. 2007.

[28] D. Iwai, S. Mihara, and K. Sato, "Extended depth-of-field projector by fast focal sweep projection," *IEEE Trans. Vis. Comput. Graphics*, vol. 21, no. 4, pp. 462–470, Apr. 2015.

[29] Z. Zhang and M. Levoy, "Wigner distributions and how they relate to the light field," in *Proc. IEEE Int. Conf. Comput. Photogr. (ICCP)*, Apr. 2009, pp. 1–10.

[30] S. B. Oh, G. Barbastathis, and R. Raskar. (2009). "Augmenting light field to model wave optics effects." [Online]. Available: https://arxiv.org/abs/0907.1545

[31] T. Cuypers, R. Horstmeyer, S. B. Oh, P. Bekaert, and R. Raskar, "Validity of wigner distribution function for ray-based imaging," in *Proc. IEEE Int. Conf. Comput. Photogr. (ICCP)*, Apr. 2011, pp. 1–9.

[32] B. M. Mout, M. Wick, F. Bociort, and H. P. Urbach, "A Wigner-based ray-tracing method for imaging simulations," *Proc. SPIE*, vol. 9630, p. 96300Z, Dec. 2015.

[33] Z. Wang, A. C. Bovik, H. R. Sheikh, and E. P. Simoncelli, "Image quality assessment: From error visibility to structural similarity," *IEEE Trans. Image Process.*, vol. 13, no. 4, pp. 600–612, Apr. 2004.

CHANG LIU received the Ph.D. degree in applied mathematics from Peking University, Beijing, China, in 2017. He is now a lecturer with the Institute of Applied Mathematics, Beijing Information Science and Technology University. His research interests include applied mathematics, computional imaging, and light field imaging.

SHAN GAO received the B.S. degree in information and computing science from the Ningbo University of Technology, Ningbo, Zhejiang, China, in 2015. She is currently pursuing the Ph.D. degree in computational mathematics with Beijing Jiaotong University, Bejing, China. Her research interests include image reconstruction and computational imaging.

XING ZHAO received the Ph.D. degree in computer science from the University of Science and Technology of China, Hefei, China. He is currently a Professor with the Beijing Advanced Innovation Center for Imaging Technology and the School of Mathematical Sciences, Capital Normal University, Beijing, China. His research interests include computerized tomography, light field imaging, and computer graphics.

JUN QIU, Ph.D., professor of mathematics, is currently the director of the Institute of Applied Mathematics, Beijing Information Science & Technology University. He also serves as the chief member of Computed Tomography Theory and Application Specialized Commission, Beijing Mathematics Society, and Ocean Optics Expert Committee of the Chinese Society for Optical Engineering. His research areas mainly include applied mathematics, signal processing, computational imaging and image reconstruction.